Calcium Activation of the Ca-ATPase Enhances Conformational Heterogeneity between Nucleotide Binding and Phosphorylation Domains†

Baowei Chen, Thomas C. Squier, and Diana J. Bigelow*

Cell Biology Group, Biological Sciences Division, Fundamental Science Directorate, Pacific Northwest National Laboratory, P.O. Box 999, Richland, Washington 99352

Received September 10, 2003; Revised Manuscript Received January 14, 2004

ABSTRACT: High-resolution crystal structures obtained in two conformations of the Ca-ATPase suggest that a large-scale rigid-body domain reorientation of approximately 50° involving the nucleotide-binding (N) domain is required to permit the transfer of the γ-phosphoryl group of ATP to Asp^{351} in the phosphorylation (P) domain during coupled calcium transport. However, variability observed in the orientations of the N domain relative to the P domain in the different crystal structures of the Ca-ATPase following calcium activation and the structures of other P-type ATPases suggests the presence of conformational heterogeneity in solution, which may be modulated by contact interactions within the crystal. Therefore, to address the extent of conformational heterogeneity between these domains in solution, we have used fluorescence resonance energy transfer to measure the spatial separation and conformational heterogeneity between donor (i.e., 5-[[2-[(iodoacetyl)amino]ethyl]amino]naphthalene-1-sulfonic acid) and acceptor (i.e., fluorescein 5-isothiocyanate) chromophores covalently bound to the P and N domains, respectively, within the Ca-ATPase stabilized in different enzymatic states associated with the transport cycle. In comparison to the unliganded enzyme, the spatial separation and conformational heterogeneity between these domains are unaffected by enzyme phosphorylation. However, calcium activation results in a 3.4 Å increase in the average spatial separation, from 29.4 to 32.8 Å, in good agreement with the 4.3 Å increase in the distance estimated from high-resolution structures where these sites are respectively separated by 31.6 Å (1IWO.pdb) and 35.9 Å (1EUL.pdb). Thus, the crystal structures accurately reflect the average solution structures of the Ca-ATPase. These results suggest that the approximation of cytoplasmic domains accompanying calcium transport, as observed from crystal structures, occurs in solution within the context of large amplitude domain motions important for catalysis. We suggest that these domain motions enhance the rates of substrate (ATP) access and product (ADP) egress and the probability of a productive juxtaposition of the γ-phosphoryl moiety of ATP with Asp^{351} on the phosphorylation domain to facilitate enzyme phosphorylation and calcium transport.

The sarco(endo)plasmic Ca-ATPase (SERCA) resequesters calcium ions following excitation−contraction coupling, which resets the calcium gradient and causes muscle relaxation, the rate-limiting step of muscle contraction (*1*). Three major SERCA isoforms of the Ca-ATPase have been identified; of these, SERCA1 is exclusively expressed in fast-twitch skeletal muscle; the most abundant source of Ca-ATPase thus has been the best characterized form of this enzyme (*2*−*4*). All of the isoforms play critical roles in calcium signaling in diverse cell types by maintaining submicromolar cytosolic calcium levels between calcium transients. As a P-type ATPase, the reaction mechanism of the Ca-ATPase is usually described in terms of two major conformations (i.e., E_1 and E_2; see Scheme 1) (*5*−*7*). In the E_1 conformation, the ATPase exposes two high-affinity calcium-binding sites to the cytoplasm. Upon occupancy of these sites, phosphorylation by Mg−ATP precedes a transition to the E_2 conformation in which these binding sites have been transformed into low-affinity sites exposed to the lumen of the sarcoplasmic reticulum (SR). After the dissociation of the calcium ions to the lumen of the SR, hydrolysis of the phosphoenzyme restores the Ca-ATPase to the E_1 conformation.

The recent solution of two high-resolution structures of the Ca-ATPase has provided considerable insight into the mechanistic basis for the long-range coupling between the sites of chemical reaction within the cytosolic domain, i.e., ATP hydrolysis and phosphoenzyme formation and sites of calcium transport within the membrane-spanning helices (*8*, *9*). These structures were obtained from the SERCA1 isoform

† This work was supported by a grant from the National Institutes of Health (HL64031).

* To whom correspondence should be addressed. E-mail: diana.bigelow@pnl.gov. Tel: (509) 376-2378.

[1] Abbreviations: AEDANS, protein-bound form of IAEDANS; $C_{12}E_8$, polyoxyethylene alcohol octaethyleneglycol *n*-monododecyl ether; EGTA, ethylene glycol bis(β-aminoethyl ether)-*N*,*N*,*N*′,*N*′-tetraacetic acid; $E_2(C_{12}E_8$ solubilized), Ca-ATPase enzyme solubilized with $C_{12}E_8$; $E_1(Ca_2)$, calcium-liganded Ca-ATPase enzyme intermediate; E(Ca free), Ca-ATPase in the presence of sufficient EGTA to sequester calcium; $E_2PO_4^-$, phosphorylated Ca-ATPase enzyme intermediate; E_2•TG, thapsigargin-bound Ca-ATPase enzyme intermediate; $E_2VO_4^-$, vanadate-bound Ca-ATPase enzyme intermediate; FITC, fluorescein 5-isothiocyanate, isomer I; FRET, fluorescence resonance energy transfer; HW, full width at half-height of a Gaussian distance distribution; IAEDANS, 5-[[2-[(iodoacetyl)amino]ethyl]amino]naphthalene-1-sulfonic acid; MES, morpholinoethanesulfonic acid; MOPS, 3-(*N*-morpholino)propanesulfonic acid; POPOP, 1,4-bis[5-phenyl-2-oxazolyl]benzene; R_0, Förster critical distance; R_{av}, average distance between donor and acceptor chromophores; SDS, sodium dodecyl sulfate; SERCA, sarco(endo)plasmic Ca-ATPase; SR, sarcoplasmic reticulum; TG, thapsigargin.

10.1021/bi0356350
Published on Web 03/05/2004

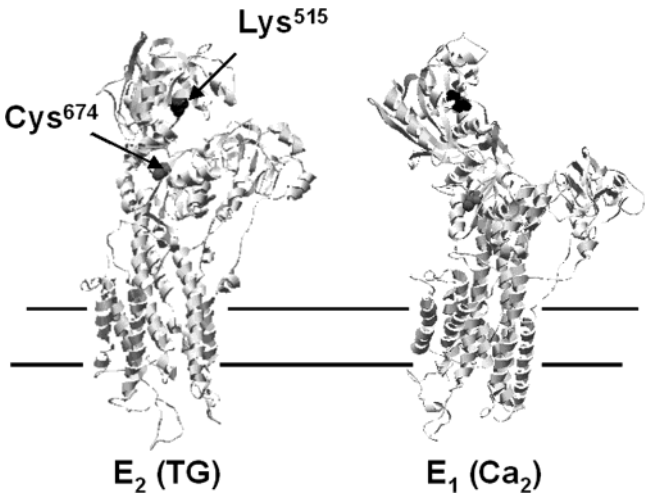

FIGURE 1: Position of Lys^{515} and Cys^{674} within the crystal structures of the fast-twitch skeletal muscle SR Ca-ATPase in the calcium-free state (E_2·TG) stabilized by TG (1IWO.pdb; left) and in the Ca^{2+}-bound state (E_1·Ca_2) (1EUL.pdb; right). The site-to-site distances measured between the α carbons is 31.6 Å within the E_2(TG) structure and increases by 4.3 Å to 35.9 Å within the E_1-(Ca_2) structure.

Scheme 1

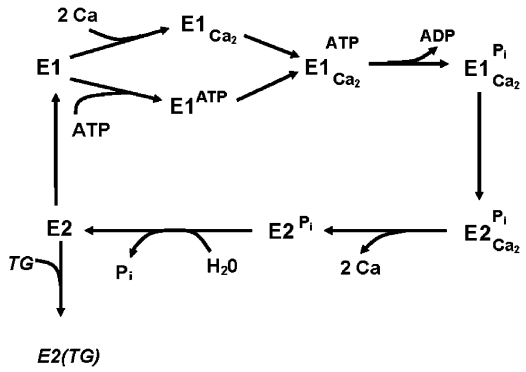

of the Ca-ATPase, isolated from rabbit fast-twitch skeletal muscle SR, crystallized in the presence of millimolar $CaCl_2$ (1EUL.pdb) or the inhibitor thapsigargin (TG) (1IWO.pdb), and result in distinct structures corresponding to $E_1(Ca_2)$ and E_2(TG) (Figure 1). Common features of these structures show three distinct cytoplasmic domains: the A domain, suggested to anchor the N domain, which binds nucleotides, and the P domain containing Asp^{351}, the residue of enzyme phosphorylation. These cytoplasmic domains connect to 10 transmembrane α helices, designated M1−M10, which contain side-by-side sites for the binding of calcium, specifically within helices, M4−M6 and M8. Comparison of these two structures indicates large-scale spatial and angular displacements of both the cytoplasmic domains and transmembrane helices during active calcium transport. Most notable is the transition between an "open" configuration with distinctly separated cytoplasmic domains in the $E_1(Ca_2)$ structure and a more compact arrangement of cytoplasmic domains in the E_2(TG) structure that has been suggested to facilitate the phosphoryl transfer of the γ−phosphoryl moiety of ATP bound within the N domain to Asp^{351} within the P domain (*10*). Thus, models of transport function commonly suggest that contact interactions between the cytosolic domains are disengaged following calcium activation (*11*). From these structural characteristics, it has been suggested that the Ca-ATPase transitions from a conformationally mobile E_1 structure to a rigid E_2 conformation, analogous to the R and T states of hemoglobin (*8*). However, the orientation of the N domain relative to the P domain exhibits variability in different crystal structures of the Ca-ATPase following calcium activation; because these differences have been suggested to result from the differences in the crystal packing forces, the precise functional significance of the large changes in the orientations of the N and P domains in the $E_1(Ca_2)$ and E_2(TG) crystal structures remains uncertain (*7*, *12*−*15*).

To address the domain movements associated with the transport mechanism of the Ca-ATPase, we used fluorescence resonance energy transfer (FRET) to measure the spatial separation between the fluorophores 5-[[2-[(iodoacetyl)-amino]ethyl]amino]naphthalene-1-sulfonic acid (IAEDANS) and fluorescein 5-isothiocyanate, isomer I (FITC), respectively covalently bound to the P and N domains of the Ca-ATPase stabilized in different enzymatic states. The intermediates that were considered in our study include the unliganded enzyme (E_2), the enzyme−calcium complex ($E1$·Ca_2), the phosphorylated enzyme intermediate (E_2−PO_4^-), and the enzyme in the presence of the phosphate analogue monovanadate (E_2−VO_4^-). Calcium binding increases the spatial separation between the P and N domains, consistent with the crystal structure. However, within each enzymatic state, there is substantial conformational heterogeneity between the probes on the P and N domains for all enzyme intermediates. Enzyme phosphorylation or vanadate binding does not alter this heterogeneity; however, calcium occupancy of the enzyme high-affinity sites results in an increased conformational heterogeneity.

EXPERIMENTAL PROCEDURES

Materials. IAEDANS was purchased from Molecular Probes (Eugene, OR); FITC and 1,4-bis[5-phenyl-2-oxazolyl]-benzene (POPOP) were obtained from Sigma Chemical Co. (St. Louis, MO). All other chemicals were reagent-grade.

Preparation of Skeletal SR Membranes. SR membranes were purified from the skeletal muscle of a rabbit as described previously with minor modifications (*16*, *17*). SR vesicles were suspended in a medium containing 0.3 M sucrose and 20 mM 3-(*N*-morpholino)propanesulfonic acid (MOPS) (pH 7.0) and were stored at −70 °C. Protein concentrations were determined by the method of Lowry and co-workers (*18*), using bovine serum albumin as a standard.

Labeling with Spectroscopic Probes. The Ca-ATPase was labeled with IAEDANS or FITC as previous described (*19*, *20*) and carried out in a medium of 20 mM MOPS (pH 6.8), 80 mM KCl, 1 mM $CaCl_2$, 5 mM $MgCl_2$, 0.4 mM IAEDANS, and 4 mg of SR protein/mL for 30 min at 25 °C. SR vesicles incubated with IAEDANS were separated from the free probe by two successive centrifugations at 100 000*g* for 45 min and resuspensions of the resulting pellet in a buffer of 0.3 M sucrose and 20 mM MOPS (pH 7.0). The Ca-ATPase was similarly labeled with FITC by incubation of SR with 40 μM FITC for 10 min at 22 °C in a medium consisting of 10 mM Tris buffer (pH 9.2), 0.1 M KCl, 0.1 mM EGTA, and 0.3 M sucrose. The stoichiometry of labeling for the probes was determined in the medium of 1% sodium dodecyl sulfate (SDS) and 0.1 M NaOH for both of the probes using the molar extinction coefficients of ϵ_{340}

$= 6100\ M^{-1}\ cm^{-1}$ and $\epsilon_{495} = 8.0 \times 10^4\ M^{-1}\ cm^{-1}$, for IAEDANS and FITC, respectively (*21*). The final labeling stoichiometries of the samples used for this paper corresponded to 5.6 ± 0.6 nmol of IAEDANS/mg of SR and 4.1 ± 0.7 nmol of FITC/mg of SR. These stoichiometries correspond respectively to the molar ratios of 1.2 ± 0.1 and 0.9 ± 0.1 probes per Ca-ATPase, based on the active Ca-ATPase concentrations measured from assays of the ATP-dependent phosphorylated enzyme (4.5 ± 0.5 nmol/mg of SR) for these SR preparations.

Buffer Conditions for Stabilization of Enzyme Intermediates. Enzyme intermediates were the result of the following buffer conditions: E(Ca_2) in 20 mM MOPS (pH 6.8), 80 mM KCl, 5 mM $MgCl_2$, 0.5 mM EGTA, and 0.6 mM $CaCl_2$ ($[Ca^{2+}]_{free} = 105\ \mu M$); E(Ca free) in 20 mM MOPS (pH 6.8), 80 mM KCl, 5 mM $MgCl_2$, and 0.5 mM EGTA; E(PO_4^-) in 10 mM Tris-MES (pH 6.0), 20 mM KH_2PO_4, 20 mM $MgCl_2$, and 1 mM EGTA ($[Ca^{2+}]_{free} = 0.5\ \mu M$); E($VO_4^-$) in 20 mM MOPS (pH 6.8), 80 mM KCl, 5 mM $MgCl_2$, 0.5 mM EGTA, and 10 μM monovanadate; E($C_{12}E_8$ soluble) in 20 mM MOPS (pH 6.8), 80 mM KCl, 5 mM $MgCl_2$, 0.5 mM EGTA, and 2 mg/mL of the detergent $C_{12}E_8$.

Steady-State Fluorescence Measurements. Fluorescence emission spectra were recorded with a FluoroMax-2 fluorometer (SPEX, Edison, NJ), using excitation and emission slits of 5 nm and exciting at 340 nm. Steady-state anisotropy (r) was calculated from the ratio of the fluorescence intensities (I) with the polarizers in the vertical (v) or horizontal (h) position

$$r = (I_{vv} - gI_{vh})/(I_{vv} + 2gI_{vh}) \quad (1)$$

where $g = I_{hv}/I_{hh}$. For IAEDANS, excitation and emission wavelengths were respectively 337 and 460 nm. For FITC, excitation and emission wavelengths were respectively 495 and 518 nm. Free calcium concentrations were determined from the total ligand and EGTA concentrations, correcting for pH and ionic conditions (*22*).

Frequency-Domain Fluorescence. Frequency-domain data were measured using an ISS K2 frequency-domain fluorometer, using a Coherent Innova argon laser with extended UV capabilities for excitation, as described previously (*23*). After the excitation at 351 nm, emitted light was detected using an Oriel interference filter centered at 460 nm, using POPOP in absolute ethanol, whose fluorescence lifetime is 1.35 ns, as a reference (*24*). The frequency-domain data were analyzed by the nonlinear least-squares method (*25*, *26*), where the time-dependent decay $I(t)$ of fluorescence was fit to a sum of exponentials

$$I(t) = \sum_{i=1}^{n} \alpha_i e^{(-t/\tau_i)} \quad (2)$$

where α_i is the preexponential factor and τ_i is the decay time. The intensity decay law is obtained from the frequency response of the amplitude-modulated light and is characterized by the frequency-dependent values of the phase shift and the extent of demodulation. The values are compared with the calculated values from an assumed decay law until a minimum of the squared deviation (χ_R^2) is obtained. The mean lifetime ($\bar{\tau}$) is directly related to the quantum yield of the fluorophore (*27*), where

$$\bar{\tau} \equiv \sum_{i=1}^{n} \alpha_i \tau_i \quad (3)$$

FRET. The intensity decay for a fluorescence donor in the presence of an acceptor permits the determination of both the average distance (R_{av}) and the width at half maximum (HW), which reflects the conformational heterogeneity of the molecule to which the donor and acceptor are bound. For example, for a single acceptor present at a distance r from a donor, the intensity decay I_{DA} (*28*) is given by

$$I_{DA}(r,t) = \sum_{i=1}^{n} \alpha_{D_i} \exp(-t/\tau_{DA_i}) \quad (4)$$

where the individual decay times observed in the presence of an energy-transfer acceptor are

$$\frac{1}{\tau_{DA_i}} = \frac{1}{\tau_{D_i}} + \frac{1}{\tau_{D_i}}\left(\frac{R_0}{r}\right)^6 \quad (5)$$

R_0 is the Förster critical distance that defines the distance where the efficiency of the resonance energy transfer is 50% for a given donor-acceptor pair. R_0 is calculated as

$$R_0 = (9.79 \times 10^3)(\kappa^2 n^{-4} Q J)^{1/6} \quad \text{(in Å)} \quad (6)$$

where κ^2 is the orientation factor, n is the refractive index, Q is the quantum yield of the donor in the absence of the acceptor, and J is the spectral overlap integral (*24*). In our experiments, the quantum yield for IAEDANS−SR was determined using quinine bisulfate as a standard ($Q = 0.54$); n was estimated to be 1.40 based on n measured for a 1 mg/mL solution of serum albumin (*29*). κ^2 was assumed to be $^2/_3$, corresponding to the random orientation between the donor and acceptor dipoles, because of the range of conformations, the possibility of rotational diffusion, and the mixed polarization of the species (*29*). The use of $\kappa^2 = {}^2/_3$ does not result in a significant error if the donor and acceptor can adopt a range of conformations. Errors in the recovered donor−acceptor separation can be estimated from a consideration of the steady-state anisotropy of both donor and acceptor chromophores; the buffer conditions used did not significantly alter the steady-state A's of bound AEDANS or FITC (*30*).

When the distance distribution is modeled as a Gaussian probability [$P(r)$], the observed intensity decay is fit as

$$I_{DA}(t) = \int_{r=0}^{\infty} P(r) \sum_{i=1}^{n} \alpha_{D_i} \exp\left[-\frac{t}{\tau_{D_i}} - \frac{t}{\tau_{D_i}}\left(\frac{R_0}{r}\right)^6\right] dr \quad (7)$$

To recover $P(r)$ from the intensity decay and minimize the number of parameters, a uniform Gaussian distribution of the donor-acceptor distances is generally assumed as

$$P(r) = \frac{1}{\sigma\sqrt{2\pi}} \exp\left[-\frac{1}{2}\left(\frac{r - R_{av}}{\sigma}\right)^2\right] \quad (8)$$

where R_{av} is the average donor−acceptor distance and σ is the standard deviation of the distribution. The width of the

distribution is reported as the full width at half-maximum (HW), given by HW = 2.354σ (*28*−*31*).

RESULTS

Selective Modification of Individual Domains of the Ca-ATPase. Direct measurements of the average spatial separation and conformational heterogeneity between individual domains of the Ca-ATPase are possible following the covalent modification of individual amino acids within these domains with donor and acceptor chromophores used for time-resolved FRET measurements. Using previously determined conditions, which are known to permit the selective modification of individual sites on the Ca-ATPase, we have covalently attached the donor AEDANS to Cys^{674} within the P domain and the acceptor FITC to Lys^{515} within the N domain of the Ca-ATPase in the SR vesicles isolated from the rabbit fast-twitch muscle (Figure 1; *19*, *20*, *32*−*34*). Several characteristics of the modified Ca-ATPase are relevant to the FRET measurements. For example, these reaction conditions modify only the Ca-ATPase as indicated from fluorescence associated exclusively with the 110 kDa Ca-ATPase protein after electrophoretic separation of the SR proteins (*35*). For this paper, SR membranes were modified at average labeling stoichiometries of 5.6 ± 0.6 nmol of AEDANS/mg of SR protein and 4.1 ± 0.7 nmol of FITC/mg of SR protein. These values correspond to the molar ratios of 1.2 ± 0.1 and 0.9 ± 0.1 for AEDANS and FITC per Ca-ATPase, respectively, based on the measurements of the Ca-ATPase concentrations in SR obtained from assays of [^{32}P]-ATP-dependent phosphoenzyme (E−P), i.e., 4.5 ± 0.5 nmol of E−P/mg of SR. Thus, the probe stoichiometries are consistent with the full labeling of all of the Ca-ATPase polypeptide chains at Cys^{674} and Lys^{515} sites, established previously by amino acid sequencing (*20*). A small extent of IAEDANS labeling may also occur at the proximal Cys^{670} positioned within 4 Å of Cys^{674}, leading to some overestimating of the conformationally heterogeneity (*36*).

The modified enzyme fully retains the ability for active calcium transport coupled to ATP hydrolysis in the case of the AEDANS-modified enzyme but requires the utilization of a smaller phosphate compound, such as acetyl phosphate, to support a calcium transport in the case of the FITC-modified Ca-ATPase. The latter requirement is a result of the occlusion of a portion of the nucleotide site by bound FITC (*37*, *38*). Thus, the ability of the AEDANS−FITC-modified Ca-ATPase to support active calcium transport demonstrates that the fluorescence measurements made with this donor−acceptor pair reflect the native conformations of the Ca-ATPase; however, the choice of FITC as an acceptor precludes the conformational measurements on the nucleotide-bound enzyme (*35*, *37*).

FRET Measurements: Steady-State Fluorescence. Steady-state measurements of fluorescence provide a convenient means to both characterize the spectral properties of bound fluorophores and estimate the mean spatial separation between the bound probes. The spatial relationship between covalently bound chromophores is estimated through the FRET measurement, which typically requires the bound probes to be located within 100 Å of one another with spectral overlap between the fluorescence emission of the donor and absorbance of the acceptor (*37*). In this respect, the fluorescence emission of AEDANS bound within the P domain of the Ca-ATPase is centered at 476 nm (Figure 2) and overlaps strongly with the absorbance spectrum of FITC centered near 495 nm, resulting in an R_0 of approximately 50 Å (*38*). In view of the distance between α carbons of Cys^{674} and Lys^{515} in the high-resolution structures of the Ca-ATPase, which are respectively 31.6 Å (E_2·TG; 1IWO.pdb) and 35.9 Å (E_1·Ca_2; 1EUL.pdb) (Figure 1), this donor−acceptor pair is optimally suited to detect alterations in the spatial separation and conformational heterogeneity between the P and N domains of the Ca-ATPase during the enzymatic cycle. After the covalent modification of Lys^{515} with FITC, there is a 39% decrease in the fluorescence intensity of AEDANS bound to Cys^{674} and an associated increase in the fluorescence at 517 nm because of the stimulated emission of FITC resulting from FRET. These results are consistent with prior FRET measurements of AEDANS- and FITC-modified Ca-ATPase (*19*, *21*, *35*, *40*).

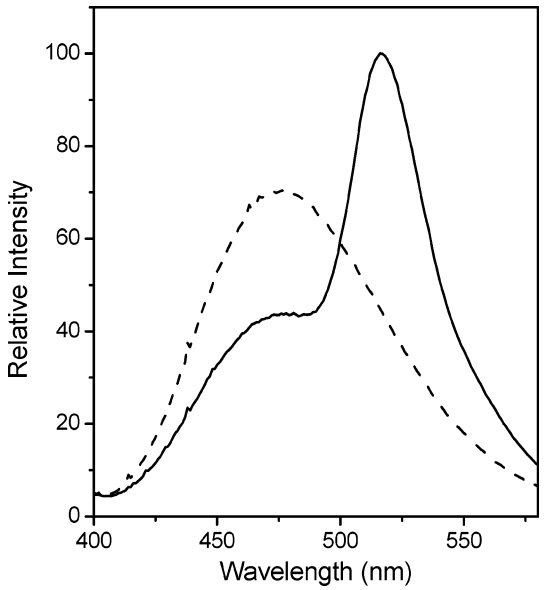

FIGURE 2: Fluorescence emission spectra demonstrating FRET between IAEDANS covalently bound to Cys^{674} in the P domain in the absence (dashed line) and presence (solid line) of FITC bound to Lys^{515} in the N domain of the Ca-ATPase. Samples consist of 100 μg of SR/mL, 20 mM MOPS (pH 6.8), 80 mM KCl, 5 mM $MgCl_2$, and 0.5 mM EGTA. Excitation was at 340 nm.

FRET from Fluorescence Lifetime Measurements. Frequency-domain fluorescence spectroscopy was used to measure the excited-state lifetime of AEDANS bound to Cys^{674} in the P domain of the Ca-ATPase in the absence and presence of FITC covalently bound to Lys^{515} in the N domain, providing a complementary method for the determination of the energy-transfer efficiencies (Figure 3). Lifetime measurements provide both sensitivity to conformational heterogeneity within proteins and, as a noncolligative property, are not prone to errors in quantitation of the probe and protein amounts. Lifetime data were collected at 20 frequencies of intensity-modulated excitation light, between 2 and 100 MHz. With increasing frequencies, a progressive increase in the phase and a decrease in the modulation of the emitted light is observed. After the covalent modification of the Ca-ATPase with FITC, the frequency response of AEDANS−Ca-ATPase is shifted to the right, indicating a reduction in the average lifetime of AEDANS as a result of FRET.

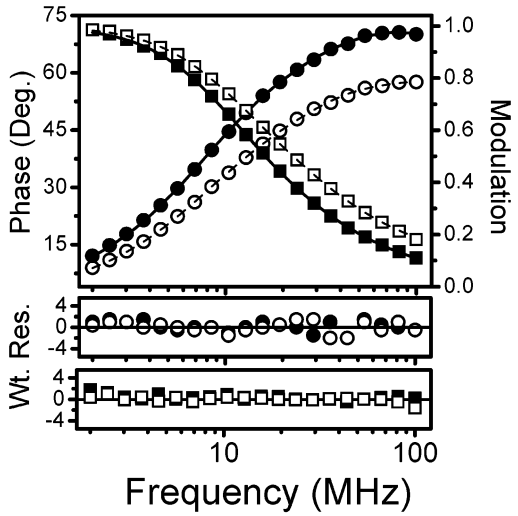

FIGURE 3: Frequency-domain lifetime data and three-exponential fits to the phase shift (●, ○) and modulation (■, □) for IAEDANS covalently bound to Cys^{674} in the P domain in the absence (●, ■) and presence (○, □) of FITC bound to Lys^{515} in the N domain of the Ca-ATPase. The solid (D) and dashed (DA) lines represent the best fits to the data. The emission decay of bound AEDANS fits best ($\chi_R^2 = 1.1$) to a three-exponential model having the lifetime components (τ_i) of 0.3, 5.6, and 18.6 ns, with respective amplitudes (α_i) of 0.57, 0.12, and 0.31; the emission decay of AEDANS−FITC is best described ($\chi_R^2 = 0.9$) by the lifetime components of 0.3, 5.5, and 17.0 ns with respective amplitudes of 0.66, 0.19, and 0.15. Measurements were made at 25 °C using 100 μg of SR/mL in 20 mM MOPS (pH 6.8), 80 mM KCl, 5 mM $MgCl_2$, and 0.5 mM EGTA. Lower panels represent the weighted residuals (i.e., the difference between the experimental data and the calculated fit divided by the experimental uncertainty) for the phase and modulation data.

For comparison with the steady-state FRET measurements, the lifetime decay data were fit as discrete exponentials. In all cases, three-exponential components are required to describe the data (as an example, see the caption to Figure 3). While the physical significance of these decay times has not been assigned, studies with other systems have demonstrated that multiple exponential lifetime decays can result from a single fluorophore site within a protein as a result of heterogeneity around the probe. This heterogeneity can result from multiple factors such as protein unfolding and other protein dynamics, probe interaction with soluble quenchers or nearby protein groups that quench the fluorophore, or rotational conformers of the fluorophore, itself (*42*−*45*). As discussed below, discrete exponential fits may not best describe the range of the conformations available to fluorophores on proteins. However, this approach to the data analysis provides a simple model that derives the mean donor lifetimes $\bar{\tau}$, in the absence and presence of the acceptor, for the determination of the energy-transfer efficiency. From this analysis, and in good agreement with the steady-state data, there is a 38% decrease in $\bar{\tau}$ because of FRET between bound AEDANS and FITC. This agreement between steady-state and lifetime-derived FRET rules out any significant donor−acceptor population within the static limit, i.e., <0.5 of R_0, where the donor fluorescence is completely quenched. Thus, possible errors in the interpretation of the FRET data are avoided.

An important additional characteristic observed from the lifetimes is that the relative decrease of $\bar{\tau}$ in the presence of FITC is unaffected by the membrane solubilization; this decrease of 39% is essentially the same as that in native membranes. Thus, the FRET between AEDANS and FITC observed for native membranes represents FRET within a single Ca-ATPase polypeptide chain with essentially no intermolecular contribution.

Rationale for the Distance Distribution Analysis. Spatial separations between protein-bound fluorophores are commonly calculated from the steady-state or lifetime FRET measurements that assume a single rigid donor−acceptor distance. However, this interpretation would seem inadequate for the Ca-ATPase, in view of the previous work demonstrating large amplitude motions of the N domain (*46*). The amplitude of these rotational motions correspond to a semiangle of approximately 44° for the unliganded enzyme, increasing by approximately 4° following calcium activation. Moreover, the rotational motion of the N domain ($\varphi_r = 5 \pm 1$ μs) is substantially longer than the fluorescence lifetime of AEDANS ($\bar{\tau} \simeq 7$ ns), ensuring the presence of the static disorder on the time scale of the FRET measurement. Thus, knowledge of this conformational heterogeneity between the Ca-ATPase domains contradicts the analysis of FRET in terms of a model that assumes a single distance and, instead, requires that the time-dependent intensity decay be fit to a model that explicitly considers a distribution of the distances. The distance distribution models have been shown to be a more appropriate description of the intramolecular donor−acceptor separations for many peptides and proteins (*6*, *24*, *29*, *31*, *47*, *48*). Moreover, the extent of conformational heterogeneity within proteins, as described by the width at half-maximum (HW) of the distance distribution, has been shown to be a more sensitive signature of the conformational changes within macromolecules than the mean donor−acceptor distance (*24*, *36*, *49*, *50*).

In the case of the present data, these two models were explicitly compared by fitting the data from IAEDANS and IAEDANS−FITC-labeled Ca-ATPase, to both of the models. The simpler Gaussian distribution model, having two floating parameters, i.e., the average recovered donor−acceptor distance (R_{av}) and the width at half-maximum of the distance distribution (HW), fits statistically as well, based on the similar goodness of fit (χ_R^2), as the single donor−acceptor-distance model derived from a model that assumes a sum of exponentials with five floating parameters (i.e., α_1, τ_1, α_2, τ_2, and τ_3; Table 1). Thus, the simpler model of the distance distribution is statistically justified.

Results from the Distance Distribution Analysis. From a consideration of the parameters obtained from an analysis of the distance distribution between the P and N domains of the Ca-ATPase, broad distance distributions are exhibited, indicating a significant degree of conformational heterogeneity (Table 1; Figures 4 and 5). The extent of conformational heterogeneity is virtually identical for E(Ca free), $E_2(PO_4^-)$, and $E_2(VO_4^-)$, where HW of these distributions are approximately 32 Å (Table 1). Under these conditions, the average spatial separation (R_{av}) between AEDANS covalently bound to Cys^{674} and FITC bound to Lys^{515} is approximately 29 Å, which is in reasonable agreement with the 31.6 Å separation between the corresponding α carbons of these amino acids in the crystal structure for E_2·TG (i.e., 1IWO.pdb). Thus, conditions used for protein crystallization have captured structures from highly populated states of an average solution structure.

Table 1: Distance Distribution Analysis of the Time-Resolved FRET Data (AEDANS−FITC)[a]

enzyme intermediate	R_0 (Å)	R_{av} (Å)	HW (Å)	χ_R^2
$E_1(Ca_2)$	48.3 ± 0.8	32.8 (32.0−34.0)	36.1 (35.4−36.8)	3.2
E(Ca free)	46.2 ± 0.6	29.4 (28.6−30.3)	32.3 (31.5−33.0)	4.9
$E_2(PO_4^-)$	47.3 ± 0.7	28.6 (27.7−29.6)	32.0 (31.3−33.0)	4.8
$E_2(VO_4^-)$	48.6 ± 1.0	28.4 (27.7−29.3)	32.8 (32.0−33.5)	5.5
$E_2(C_{12}E_8$ soluble)	54.7 ± 0.8	45.4 (43.9−46.8)	56.8 (55.0−58.7)	2.5

[a] The values of the average donor−acceptor distance (R_{av}) and the width of the distribution as the full width at half-maximum (HW) are derived from a global fitting of the data. Values in parentheses indicate the respective values of R_{av} or HW at one standard deviation from the mean (also see Figure 4). R_0 is the Förster critical distance, i.e., where the energy transfer is 50%; the values represent the mean and standard errors for 2 or 3 samples for each buffer condition. Enzyme intermediates were stabilized by the following buffer conditions: $E(Ca_2)$ in 20 mM MOPS (pH 6.8), 80 mM KCl, 5 mM $MgCl_2$, 0.5 mM EGTA, and 0.6 mM $CaCl_2$ ($[Ca^{2+}]_{free}$ = 105 μM); E(Ca free) in 20 mM MOPS (pH 6.8), 80 mM KCl, 5 mM $MgCl_2$, and 0.5 mM EGTA; $E(PO_4^-)$ in 10 mM Tris-MES (pH 6.0), 20 mM KH_2PO_4, 20 mM $MgCl_2$, and 1 mM EGTA ($[Ca^{2+}]_{free}$ = 0.5 μM); $E(VO_4^-)$ in 20 mM MOPS (pH 6.8), 80 mM KCl, 5 mM $MgCl_2$, 0.5 mM EGTA, and 10 μM monovanadate; $E(C_{12}E_8$ soluble) in 20 mM MOPS (pH 6.8), 80 mM KCl, 5 mM $MgCl_2$, 0.5 mM EGTA, and 2 mg/mL of the detergent $C_{12}E_8$.

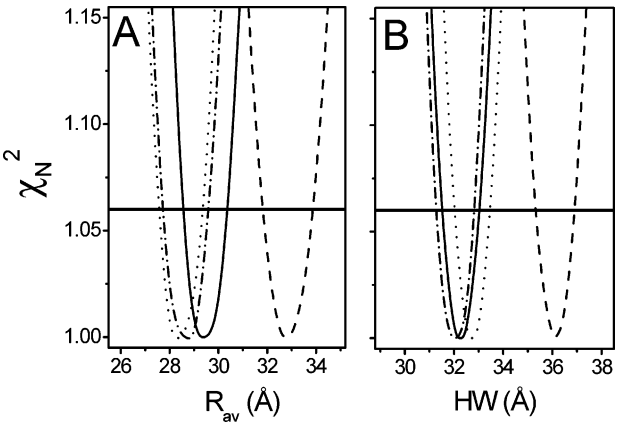

FIGURE 4: Depiction of the error surfaces demonstrating the calcium-induced increase in (panel A) the average donor−acceptor separation (R_{av}) and (panel B) conformational heterogeneity (HW) between the P and N domains of the Ca-ATPase. Error surfaces were constructed by incrementally adjusting either R_{av} or HW and allowing all other parameters to vary in the least-squares analysis (Beechem et al., 1991), where the goodness of fit (χ_R^2) was normalized to 1.0, i.e., (χ_N^2). The horizontal line corresponds to the *F* statistic for 1 standard deviation. Thus, the error surfaces that do not overlap at the level of the *F* statistic are considered statistically different. Experimental conditions are described in the footnote of Table 1, corresponding to $E_1(Ca_2)$ (dashed line), E(Ca free) (solid line), $E_2(PO_4^-)$ (dash−dotted line), and $E_2(VO_4^-)$ (dotted line).

Calcium activation results in an increase in both R_{av} and HW, which increase by 3.4 Å and 3.8 Å, respectively (Table 1). Similar increases in R_{av} of 4.2 and 4.4 Å are observed for $E_2(PO_4^-)$ and $E_2(VO_4^-)$, respectively. These increases in the average spatial separation are consistent with the crystal structure for $E_1{\cdot}Ca_2$ (1EUL.pdb), where the average spatial separation between these sites increases by 4.3 Å in comparison to that of $E_2{\cdot}TG$. To assess the significance of these differences, an error surface analysis was performed

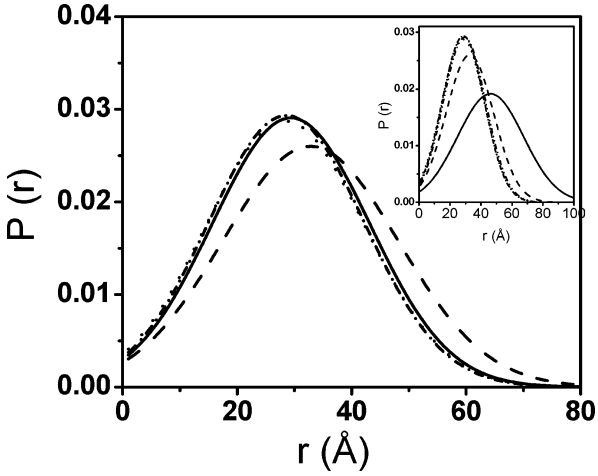

FIGURE 5: Increased conformational heterogeneity between the P and N domains of the Ca-ATPase following calcium activation. Graphical depiction of the peak-normalized Gaussian distance distributions depicting the relationship between the fractional population of the donor−acceptor distances $P(r)$ and spatial separation (r) between IAEDANS covalently bound to Cys^{674} in the P domain and the presence of FITC covalently bound to Lys^{515} in the N domain of the Ca-ATPase. Experimental conditions are described in the footnote of Table 1, corresponding to $E_1(Ca_2)$ (dashed line), E(Ca free) (solid line), $E_2(PO_4^-)$ (dash-dotted line), $E_2(VO_4^-)$ (dotted line). The inset shows this same data in comparison with the $E_2(C_{12}E_8$ solubilized) sample (solid line), illustrating the increased heterogeneity induced by the loss of bilayer stabilization.

on the time-resolved FRET data. This involved fitting the data by incrementally adjusting either the R_{av} or HW values (Figure 4A or B, respectively) and allowing all other parameters to vary in the least-squares analysis, where the resulting goodness of fit, expressed as the χ^2 value, was normalized to 1.0. The curves generated show a minimum χ^2 value (1.0) for the best fit. The horizontal line indicates one standard deviation. Thus, distributions whose error surfaces overlap in the region below the line are not significantly different. The lack of overlap in the error surfaces confirms the statistical significance of the distinction between the E_2 and $E_1{\cdot}Ca_2$ conformations of the Ca-ATPase in both of the R_{av} and HW parameters; conversely, E(Ca free), $E_2(PO_4^-)$, and $E_2(VO_4^-)$ are not different. These results indicate that the observed structural changes apparent in the crystal structures accurately reflect the average structures in solution and are not distorted by the intermolecular crystal-packing forces. The 3.8 Å increase in HW upon calcium activation is likewise consistent with direct measurements of the dynamics of the N domain, which indicate large amplitude motions of the N domain, whose semiangle increases by approximately 4° from 44° to 48° upon calcium activation (*46*).

As a further point of reference for the recovered values of R_{av} and HW of the Ca-ATPase in the native SR membranes, we have measured these parameters after subjecting the Ca-ATPase to a mild structural perturbation induced by solubilization with the detergent $C_{12}E_8$. This treatment eliminates the stabilizing influence of the intact bilayer but retains the layer of native lipids that associate directly with the membrane-spanning region of the ATPase resulting in a decrease (∼40%) in the enzyme activity (Figure 5; Table 1). Under these solubilizing conditions there is a substantially increased conformational heterogeneity as

evidenced by a recovered HW of 56.8 Å and an increase in the spatial separation between AEDANS at Cys^{674} and FITC at Lys^{515} (R_{av} = 45.4 Å). This result is consistent with the role of the intact bilayer in stabilizing the protein structure and in orienting the relative positions of the P and N domains. The Ca-ATPase is thus similar to other integral membrane proteins, in which this stabilization of cytosolic domains through their linkage to transmembrane helices permits a substantial degree of conformational heterogeneity without the need for strong stabilizing interactions between the protein domains in soluble proteins (*51*). Indeed, the crystal structures of the Ca-ATPase suggest few interdomain contact interactions between the cytosolic domains, consistent with the large amplitude motion of the N domain (*7*). While available information regarding the $C_{12}E_8$ effects does not allow the possiblility of direct interactions of the detergent in the proximity of the probe sites, it should be noted that the structural changes induced by $C_{12}E_8$ are in marked contrast with the dramatic increases in recovered HW (up to ~80 Å) previously measured for AEDANS−FITC−Ca-ATPase after denaturation in 5 M urea (*35*).

DISCUSSION

Summary of the Results. The average spatial separation between the P and N domains for the Ca-ATPase in native SR membranes and the calcium-dependent increase (3.4 Å) in their spatial separation are essentially identical to those observed in the high-resolution crystal structures. These results indicate that the high-resolution crystal structures accurately reflect the average solution structures of the Ca-ATPase in the native SR membranes (*8*, *9*) and that the crystal-contact interactions between domain elements under these conditions do not appreciably distort the relative orientations of the cytosolic domains. Moreover, the time-resolved FRET measurements for the membrane-bound Ca-ATPase indicate a considerable extent of conformational heterogeneity between the P and N domains, as evidenced by measured HWs ranging from 32 to 36 Å for all membrane-bound enzyme intermediates examined (Table 1). These results suggest that the interconversion between the heterogeneous enzyme states functions to favor the probability of forming a productive enzyme intermediate to facilitate catalysis, as opposed to acting as a structural switch to induce the formation of a discrete enzyme state.

Calcium Activation and the Reaction Mechanism of the Ca-ATPase. Conformational changes associated with the sequential binding of two calcium ions at sites near the bilayer center favor catalytic activation and ATP utilization to form a phosphoenzyme intermediate involving Asp^{351} located approximately 50 Å from the calcium sites (*52*). Detailed kinetic analysis has revealed that binding of the first calcium induces the reorientation of transmembrane elements to form a second calcium binding site, whose occupancy promotes the formation of the phosphoenzyme (*53*). After phosphoenzyme formation, calcium liganding is disrupted, favoring the vectorial transport of calcium into the SR lumen. Thus, calcium activation and the long-range structural coupling between the transmembrane elements and cytosolic domains are of primary importance to the mechanism of calcium transport. From the crystal structures of the Ca-ATPase, it is apparent that calcium binding is associated with the formation of a more open structure of the cytoplasmic domains with respect to one another (Figure 1) (*8*, *9*). On the other hand, with the exception of the transmembrane elements, calcium binding causes minimal structural changes within individual domains (*7*). Thus, it is commonly suggested that calcium activation induces the rigid-body domain movements that disengage the contact interactions between the P and N domains, creating a more relaxed structure that facilitates nucleotide binding (*9*−*11*).

Measurements of conformational heterogeneity between the P and N domains provide a direct assessment of these structural predictions (Figure 5). Before calcium activation, the average spatial separation between the P and N domains and the extent of conformational heterogeneity are virtually identical for the Ca-ATPase stabilized in various enzyme states, [E_2−PO_4^-, E_2−VO_4^-, or E(EGTA)] (Table 1), indicating that these states have the same range of available conformations (Table 1; Figures 4 and 5). After calcium occupancy of the high-affinity sites (E_1·Ca_2), there is a unique increase in both the average donor−acceptor distance (R_{av}) and its conformational heterogeneity (HW), consistent with the more open nature of this conformation in the crystals. Thus, these results support previous suggestions that the Ca-ATPase transport mechanism involves global structural transitions between the two major conformational states (i.e., E_1 and E_2) that modulate the long-range conformational coupling between the formation of the phosphoenzyme intermediate and high-affinity calcium binding (*5*). However, the extent of conformational heterogeneity is large for both states (Table 1; Figure 5), suggesting that there are no long-lived interactions between the N domain and other domain elements of the Ca-ATPase. These results rule out models that require stabilizing interdomain interactions to favor phosphoryl transfer. Rather, these results support earlier suggestions regarding the presence of a flexible hinge sensitive to calcium activation (*46*).

Furthermore, the extent of conformational heterogeneity in both the calcium-bound and calcium-free conformations is consistent with previous kinetic measurements demonstrating that calcium activation does not significantly affect the kinetics of ATP association with the Ca-ATPase (*54*, *55*). Likewise, ATP binding has essentially no effect on the kinetics of calcium association or the dynamics of the N domain (*46*, *56*). In fact, calcium and ATP bind to the Ca-ATPase by a random mechanism.

Domain Movements and Mechanism of Calcium Transport. From the available high-resolution structures of the Ca-ATPase, it is apparent that large movements of the domains with respect to one another are essential to the transport function (*7*−*9*, *15*). Moreover, the extent of the conformational heterogeneity present between the P and N domains indicates that these movements cannot be ascribed to discrete rigid-body movements. Rather, Brownian motions of domains, which have previously been shown to be rate limiting under a variety of physiological conditions that alter both motions and transport activity, are likely to play an important functional role (*57*−*62*). Specifically, we hypothesize that motions of the flexible N domain, and possibly of the P domain facilitate the juxtaposition of bound ATP within the N domain and Asp^{351} within the P domain. The fact that the occupancy of the high-affinity calcium sites increases the amplitude of the N domain motion (*46*) and the extent of conformational heterogeneity between the P and N

domains suggests that the calcium-directed Brownian diffusion facilitates the phosphoryl-transfer reaction. Given that the rate of diffusion of the N domain (approximately 10^4 s^{-1}) is about 50-fold faster than the rate of phosphoenzyme formation following ATP and calcium activation (approximately 200 s^{-1}), it is apparent that the productive association between the P and N domains involves a poorly populated transition state for this partial reaction that is the result of directed Brownian diffusion (*15*, *46*, *63*, *64*).

This interpretation is consistent with the observation that there are minimal contact interactions between the cytosolic domains and follows from the structural constraints imposed on membrane proteins by the thermodynamically stable transmembrane region (*51*). Thus, the orientation and proximity of cytosolic domains are defined by the relative organization of the transmembrane helices. These constraints permit the coordinated movement of the cytosolic domains, without the requirement for interdomain-stabilizing interactions common in soluble proteins that catalyze chemical transformations. Indeed, previous measurements confirm the importance of large-amplitude domain motions in energy transducing systems and, with respect to the Ca-ATPase domain motions of the N domain, have previously been shown to be catalytically important (*46*, *65*−*71*). Indeed, the physiological modulators of Ca-ATPase function, involving phospholamban expression and alterations in lipid composition, directly modulate activity through the modulation of the N domain dynamics (*62*, *72*, *73*).

Conclusions and Future Directions. We report that the average orientations of the P and N domains with respect to one another in biological membranes are essentially identical to those depicted in the high-resolution crystal structure for the apo- and calcium-activated forms of the Ca-ATPase, reaffirming the reported importance of the large-domain movements for the N domain upon calcium activation. However, these average structures need to be viewed in the context of large-amplitude movements, because there is considerable conformational heterogeneity with respect to the orientation of the P and N domains irrespective of the enzyme state. Thus, these results suggest a considerable overlap with respect to the orientations of the cytosolic domains of the Ca-ATPase in different enzymatic states and that catalysis involves the formation of the transition states involving a subpopulation of the total enzyme. Additional understanding of the relationship between the various conformations of the Ca-ATPase and the reaction mechanism will require the investigation of the coordinated movements of the P, N, and A domains of the Ca-ATPase during the reaction cycle to identify the possible concerted domain movements that may function to couple the lattice and to coordinate the motions associated with enzyme phosphorylation and hydrolysis that mediate the vectorial transport of calcium.

REFERENCES

1. Ruegg, J. C. (1992) *Calcium in Muscle Contraction*, pp 52−53, Springer-Verlag, New York.
2. MacLennan, D. H., Brandl, C. J., Korczak, B., and Green, N. M. (1985) *Nature 316*, 696−700.
3. Wu, K. D., Lee, W. S., Wey, J., Bungard, D., and Lytton, J. (1985) *Am. J. Physiol. 269*, C774−C784.
4. Bilmen, J. G., Khan, S. Z., Javed, M. H., and Michelangeli, F. (2001) *Eur. J. Biochem. 268*, 6318−6327.
5. de Meis, L., and Vianna, A. L. (1979) *Annu. Rev. Biochem. 48*, 275−292.
6. Lutsenko, S., and Kaplan, J. H. (1995) *Biochemistry 34*, 15607−15613.
7. Stokes, D. L., and Green, N. M. (2003) *Annu. Rev. Biophys. Biomol. Struct. 32*, 445−468.
8. Toyoshima, C., Nakasoko, M., Nomura, H., and Ogawa, H. (2000) *Nature 405*, 647−655.
9. Toyoshima, C., and Nomura, H. (2002) *Nature 418*, 605−611.
10. Green, N. M., and MacLennan, D. H. (2002) *Nature 418*, 598−599.
11. Hilge, M., Siegel, G., Vuister, G. W., Guntert, P., Gloor, S. M., and Abrahams, J. P. (2003) *Nat. Struct. Biol. 10*, 468−474.
12. Zhang, P., Toyoshima, C., Yonekura, K., Green, N. M., and Stokes, D. L. (1998) *Nature 392*, 835−839.
13. Ogawa, H., Stokes, D. L., Sasabe, H., and Toyoshima, C. (1998) *Biophys. J. 75*, 41−52.
14. Rice, W. J., Young, H. S., Martin, D. W., Sachs, J. R., and Stokes, D. L. (2001) *Biophys. J. 80*, 2187−2197.
15. Xu, C., Rice, W. J., Wanzhong, H., and Stokes, D. L. (2002) *J. Mol. Biol. 316*, 201−211.
16. Fernandez, J. L., Rosemblatt, M., and Hidalgo, C. (1980) *Biochim. Biophys. Acta 599*, 552−568.
17. Ferrington, D. A., Reijneveld, J. C., Bär, P. R., and Bigelow, D. J. (1996) *Biochim. Biophys. Acta 1279*, 203−213.
18. Lowry, O. H., Rosebrough, N. J., Farr, A. L., and Randall, R. J. (1951) *J. Biol. Chem. 193*, 265−275.
19. Bigelow, D. J., Squier, T. C., and Inesi, G. (1992) *J. Biol. Chem. 267*, 6952−6962.
20. Wawrzynow, A., Collins, J. H., and Coan, C. (1993) *Biochemistry 32*, 10803−10811.
21. Squier, T. C., Bigelow, D. J., Garcia de Ancos, J., and Inesi, G. (1987) *J. Biol. Chem. 262*, 4748−4754.
22. Fabiato, A. (1988) *Methods Enzymol. 157*, 378−417.
23. Hunter, G. W., and Squier, T. C. (1998) *Biochim. Biophys. Acta 1415*, 63−76.
24. Lakowicz, J. R. (1999) *Principles of Fluorescence Spectroscopy*, 2nd ed., pp 395−406, Kluwer Academic/Plenum Publishers, New York.
25. Gratton, E., Lakowicz, J. R., Maliwal, B., Cherek, H., Laczko, G., and Limkeman, M. (1984) *Biophys. J. 46*, 479−486.
26. Lakowicz, J. R., and Keating-Nakamoto, S. (1984) *Biochemistry 23*, 3013−3021.
27. Luedkte, R., Owen, C. S., Vanderkooi, J. M., and Karush, F. (1981) *Biochemistry 20*, 2927−2936.
28. Fairclough, R. H., and Cantor, C. R. (1978) *Methods Enzymol. 48*, 347−379.
29. Haas, E., Katchalski-Katzir, E., and Steinberg, I. Z. (1978) *Biochemistry 17*, 5064−5070.
30. Wu, P., and Brand, L. (1992) *Biochemistry 31*, 7939−7947.
31. Cheung, H. C. (1991) in *Topic in Fluorescence Spectroscopy* (Lakowicz, J. R., Ed.) Vol. 2, pp 128−176, Plenum Press, New York.
32. Kubo, K., Suzuki, H., and Kanazawa, T. (1990) *Biochim. Biophys. Acta 1040*, 251−259.
33. Hua, S., Fabris, D., and Inesi, G. (1999) *Biophys. J. 77*, 2217−2225.
34. Fonseca, M. M., Scofano, H. M., Carvalho-Alves, P. C., Barrabin, H., and Mignaco, J. A. (2002) *Biochemistry 41*, 7483−7489.
35. Chen, B., Jones, T. E., and Bigelow, D. J. (1999) *Biochemistry 38*, 14887−14896.
36. Bishop, J. E., Squier, T. C., Bigelow, D. J., and Inesi, G. (1988) *Biochemistry 27*, 5233−5240.
37. Mitchinson, C., Wilderspin, A. F., Trinnaman, B. J., and Green, N. M. (1982) *FEBS Lett. 146*, 87−92.
38. Teruel, J. A., and Inesi, G. (1988) *Biochemistry 27*, 5885−5890.
39. Stryer, L. (1978) *Annu. Rev. Biochem. 47*, 819−846.
40. Förster, T. (1948) *Annu. Phys. (Leipzig) 2*, 55−75. Translated by R. S. Knox.
41. Birmachu, W., Nisswandt, F. L., and Thomas, D. D. (1989) *Biochemistry 28*, 3940−3947.
42. Eftink, M. R., Ghiron, C. A., Kautz, R. A., and Fox, R. O (1989) *Biophys. J. 55*, 575−579.
43. Dahms, T. E. S., Willis, K. J., and Szabo, A. G. (1995) *J. Am. Chem. Soc. 117*, 2321−2326.
44. Tanaka, F., and Mataga, N. (1987) *Biophys. J. 51*, 487−495.
45. Alcala, J. R. (1994) *J. Chem. Phys. 101*, 4578−4584.
46. Huang, S., and Squier, T. C. (1998) *Biochemistry 37*, 18064−18073.

47. Sun, H., Yin, D., Coffeen, L. A., Shea, M. A., and Squier, T. C. (2001) *Biochemistry 40*, 9605−9617.
48. Chen, B., and Bigelow, D. J. (2002) *Biochemistry 41*, 13965−13972.
49. Yao, Y., and Squier, T. C. (1996) *Biochemistry 35*, 6815−6827.
50. She, M., Xing, J., Dopng, W. J., Umeda, P. K., and Cheung, H. (1998) *Biochemistry 36*, 6754−6751.
51. White, S. H., and Wimley, W. C. (1999) *Annu. Rev. Biophys. Biomol. Struct. 28*, 319−365.
52. Bigelow, D. J., and Inesi, G. (1992) *Biochim. Biophys. Acta 1113*, 323−338.
53. Inesi, G., Zhang, Z., and Lewis, D. (2002) *Biophys. J. 83*, 2327−2332.
54. Teruel, J. A., Kurzmack, M., and Inesi, G. (1987) *J. Biol. Chem. 262*, 13055−13060.
55. Reinstein, J., and Jencks, W. P. (1993) *Biochemistry 32*, 6632−6642.
56. Fernandez-Belda, F., Garcia-Carmona, F., and Inesi, G. (1988) *Arch. Biochem. Biophys. 260*, 118−124.
57. Bigelow, D. J., Squier, T. C., and Thomas, D. D. (1986) *Biochemistry 25*, 194−202.
58. Squier, T. C., and Thomas, D. D. (1988) *J. Biol. Chem. 263*, 9171−9177.
59. Squier, T. C., Bigelow, D. J., and Thomas, D. D. (1988) *J. Biol. Chem. 263*, 9178−9186.
60. Squier, T. C., Hughes, S. E., and Thomas, D. D. (1988) *J. Biol. Chem. 263*, 9162−9170.
61. Negash, S., Chen, L. T., Bigelow, D. J., and Squier, T. C. (1996) *Biochemistry 35*, 11247−11259.
62. Negash, S., Huang, S., and Squier, T. C. (1999) *Biochemistry 38*, 8150−8158.
63. Petithory, J. R., and Jencks, W. P. (1988) *Biochemistry 27*, 8626−8635.
64. Inesi, G., and de Meis, L. (1989) *J. Biol. Chem. 264*, 5929−5936.
65. Kinosita, K., Ishiwata, S., Yoshimura, H., Asai, H., and Ikegami, A. (1984) *Biochemistry 23*, 5963−5975.
66. Lesk, A., and Chothia, C. (1988) *Nature 335*, 188−190.
67. Prochniewicz, E., Zhang, Q., Howard, E. C., and Thomas, D. D. (1996) *J. Mol. Biol. 255*, 446−457.
68. Gerstein, M., and Chothia, C. (1999) *Science 285*, 1682−1683.
69. Ito, K., Uyeda, T., Suzuki, Y., Sutoh, K., and Yamamoto, K. (2003) *J. Biol. Chem. 278*, 31049−31057.
70. Huang, Y., Lemieux, M. J., Song, J., Auer, M., and Wang, D.-N. (2003) *Science 301*, 616−620.
71. Abramson, J., Smirnova, I., Kasho, V., Verner, G., Kaback, H. R., and Iwata, S. (2003) *Science 301*, 610−615.
72. Hunter, G. W., Bigelow, D. J., and Squier, T. C. (1999) *Biochemistry 38*, 4604−4612.
73. Hunter, G. W., Negash, S., and Squier, T. C. (1999) *Biochemistry 38*, 1356−1364.

BI0356350